

Theoretical Study of Plasmonic Lasing in Junctions with many Molecules

Yuan Zhang,^{1,*} Klaus Mølmer,^{1,†} and Volkhard May^{2,‡}

¹*Department of Physics and Astronomy, Aarhus University, Ny Munkegade 120, DK-8000 Aarhus C, Denmark*

²*Institute für Physik, Humboldt-Universität zu Berlin, Newtonstraße 15, D-12489 Berlin, Germany*

We calculate the quantum state of the plasmon field excited by an ensemble of molecular emitters, which are driven by exchange of electrons with metallic nano-particle electrodes. Assuming identical emitters that are coupled collectively to the plasmon mode but are otherwise subject to independent relaxation channels, we show that symmetry constraints on the total system density matrix imply a drastic reduction in the numerical complexity. For N_m three-level molecules we may thus represent the density matrix by a number of terms scaling as $(N_m + 8)!/(8!N_m!)$ instead of 9^{N_m} , and this allows exact simulations of up to $N_m = 10$ molecules. Our simulations demonstrate that many emitters compensate strong plasmon damping and lead to the population of high plasmon number states and a narrowed linewidth of the plasmon field. For large N_m , our exact results are reproduced by an approximate approach based on the plasmon reduced density matrix. With this approach, we have extended the simulations to more than 50 molecules and shown that the plasmon number state population follows a Poisson-like distribution. An alternative approach based on nonlinear rate equations for the molecular state populations and the mean plasmon number also reproduce the main lasing characteristics of the system.

PACS numbers: 33.80.-b, 68.65.-k, 05.60.Gg, 85.65.+h

I. INTRODUCTION

Hybrid systems of metal nano-particles (MNP) and molecular quantum emitters have attracted increased attention in the last two decades [1, 2]. In particular, nonlinear effects, related to the quantum nature of (surface) plasmons, i.e. collective oscillation of conduction band electrons in the MNP offer interesting lasing effects in the so-called plasmonic nano-laser [3–14]. Rather than the radiation mode in a normal laser cavity, the plasmonic nano-laser utilizes a confined plasmon oscillation. Since the size of the nano-laser can be much smaller than the wavelength of the light generated by the plasmon, the optical diffraction limit restricting the size of conventional laser does not apply for the plasmonic nano-laser [15].

The rapid damping of plasmon excitations impedes the achievement of plasmonic lasing [16] unless many quantum emitters concertedly transfer their energy to the MNP. These quantum emitters should, in turn be excited, e.g., by optical pumping [3–12] or by electrical injection [13, 14]. In Ref.[17], we proposed several approaches to describe the optically pumped plasmonic nano-laser, noting that the analyses can be readily extended to the electrically pumped nano-laser [18].

To compensate the plasmon damping and to realize strong plasmon excitation, we can either increase the excitation strength or the number of quantum emitters. The increased strength raises the excited state probability of the emitters, which enables them to transfer energy more efficiently to the MNP. However, it may be hard to realize in experiments with a single emitter. If we turn to many quantum emitters, their mutual coupling can lead to the formation of exciton states, which may have different transition energies compared to that

of the isolated quantum emitters, i.e. inhomogeneous broadening [19]. As a result, the energy transfer from the quantum emitters to the MNP plasmon becomes inefficient, and the coupling to other plasmon modes may occur, which further complicates the situation [16].

In this work we aim to prove the principle of plasmonic lasing with an idealized system, where many identical and non-interacting quantum emitters couple with one plasmon mode. This ideal system has been studied with non-linear rate equations [15, 20–24], with a Fokker-Planck equation [25] as well as with a reduced density matrix equation (RDM) [17, 26]. In most studies, the quantum emitters are treated as two-level systems incoherently driven by an effective pump. Although this effective description can capture the main physics of the systems, it is unable to describe the real experiments. For example, the optical pumping utilized in Ref. [3–5, 9] relies on two processes: a laser excitation of the quantum emitters to a higher excited state and a subsequent decay to a lower excited state. The electrical injection applied in Ref. [13, 14] also requires the participation of intermediate electron states.

To go beyond the effective description, the theories developed so-far should be extended and the quantum emitters should be treated as multi-levels systems. Fortunately, the theory presented in [17] can be easily extended to three-level systems. Such an extension will be elaborated in the present article. In particular, the numerical exact method to solve RDM equations, which was initially proposed by M. Richter and A. Knorr in [26] for many identical two-levels systems coupled to a cavity or plasmon mode, can be easily extended to the case of many identical multi-levels systems. This method actually provides another way to solve the dissipative Cavity-QED problem without using Dicke states [29] and therefore can be utilized to study many related problems, for example, sub-radiance and super-radiance [32], lasing [30, 31], and collective behavior of spin-ensembles [33–35].

In the present article, we apply the extended theory to an electrically pumped molecular junction, cf. Fig.1(a), and demonstrate that a laser with electrically pumped dye

* yzhang@phys.au.dk

† moelmer@phys.au.dk

‡ may@physik.hu-berlin.de

molecules is theoretically possible. Our study may also contribute to the exploration of plasmon lasers with an electrically pumped organic semiconductor layer, cf. Fig.1(b). More processes are involved, for example interlayer electron-transfer, exciton formation etc., and the modeling of such a structure is beyond the scope of the present article. If realized, however, this kind of laser may replace the relative expensive semiconductor laser and may thus have strong impact on the industry [27, 28].

The article is organized as follows. In Sec. II, we introduce the model of the junction system. In Sec. III, we present a general RDM approach to solve the system dynamics, the electric current signal and the optical emission spectrum. This approach was previously used to simulate junctions with up to 5 molecules in [18]. In Sec. IV, we develop an approach for junctions with identical molecules, which all couple coherently to the plasmon mode but decay and decohere independently. The symmetry of the RDM is explored to drastically reduce the computational effort, and simulations are carried out for junctions with up to 10 molecules. In Sec. V, we eliminate the molecular degrees of freedom and introduce and solve an approximate master equation for the plasmon RDM, which readily applies for junctions with up to 50 molecules. In Sec. VI, we eliminate instead the plasmon state and obtain non-linear equations for the molecular RDM. This approach allows calculation of the mean plasmon number which we compare with the results obtained by the other methods. The paper ends with several concluding remarks and an outlook in Sec. VII.

II. MOLECULAR JUNCTION MODEL

The molecular junction, formed by many molecules suspended between two metallic leads, is shown in Fig.1 (a). The left lead with a spherical form can support plasmon excitations, and we assume that one of its plasmon modes is resonant with a molecular transition. The right cavity-shaped lead may also support plasmon excitations, which, we assume, are far off-resonance with the left lead plasmon and the molecules. The molecules are placed between the two leads and are well separated from each other so that their excitonic coupling can be ignored. We assume that their transition dipole moments are tangential to the surface of the left lead and that they couple resonantly with same strength to one single plasmon mode. Similar assumptions may be valid for layer configurations, cf. Fig.1 (b).

The theoretical description of the junction follows Ref. [18]. The molecular Hamiltonian reads

$$H_{\text{mol}} = \sum_{n=1}^{N_m} \sum_{a_n} E_{na} |a_n\rangle \langle a_n|. \quad (1)$$

Here, N_m is the number of molecules, and a_n denotes the electronic state of the n^{th} molecule. The set of relevant states includes the ground state $a_n = g_n$ and the excited state $a_n = e_n$ of the neutral molecule, as well as the negatively charged molecular (ground) state $a_n = f_n$, cf. Fig.1 (c). The transition dipole moment of the neutral molecules is $\mathbf{d}_n = d_{\text{mol}} \mathbf{e}_n$.

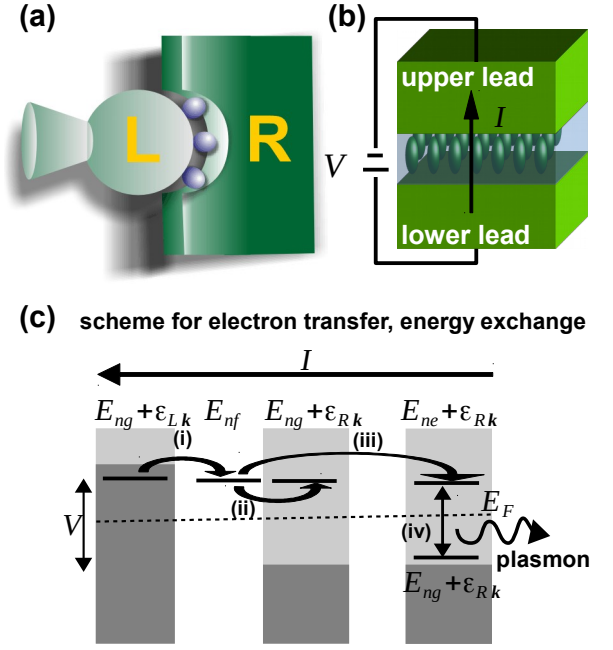


Figure 1. The physical system consists of molecules sandwiched between a spherical left lead supporting plasmon excitations and a right hollow lead, cf. panel (a). Panel (b) shows an alternative system with an organic semiconductor layer sandwiched between two metallic layers, supporting cavity plasmons between the layers. Schematic panel (c): light (dark) gray areas indicate unoccupied (occupied) electron states of the electrodes; boundaries of the areas are Fermi energies; the dashed line indicates the Fermi energies at zero-applied voltage. Energy conservation, cf. Eq. (8), requires: for charging process (i), energy of neutral molecule (ground state) plus that of electrons of the left lead $E_{ng} + \epsilon_{Lk}$ is identical to energy of charged molecule E_{nf} ; for discharge processes (ii) and (iii), the energy E_{nf} is equal to that of neutral molecule (excited or ground state) plus that of unoccupied electron states of the right lead $E_{ne} + \epsilon_{Rk}$ or $E_{ng} + \epsilon_{Rk}$ (shown separately for clarity); process (iv) shows energy exchange with the left lead plasmon.

The dipole plasmons of the left spherical lead can be modeled as three degenerate quantum harmonic oscillators [44] with the Hamiltonian

$$H_{\text{pl}} = \sum_I \hbar \omega_{\text{pl}} C_I^+ C_I. \quad (2)$$

Here, C_I^+ and C_I are creation and annihilation operator of the plasmon excitations with excitation energy $\hbar \omega_{\text{pl}}$ (the ground-state energy is defined to be zero). We choose the plasmon modes such that the plasmon dipole moments read $\mathbf{d}_I = d_{\text{pl}} \mathbf{e}_I$, where \mathbf{e}_I are Cartesian unit vectors $I = x, y, z$. There is a further infinite set of multipole plasmon oscillators, which however are not resonant with the molecules and are hence omitted from our analysis, cf. the discussion in Ref. [17, 18].

The plasmons get excited by a resonant energy exchange with the molecular emitters, which in turn are excited through an electron transfer between the leads and the molecules [36, 37], cf. Fig.1 (c). Note that this differs from the non-resonant plasmon excitation through direct, inelastic electron

transfer between metallic leads [38]. We assume that the electron transfer is weak and that the coupling of the molecular states to the electron continuum states in the leads can be treated by a master equation approach, see below. The resonant energy exchange coupling is described by

$$H_{\text{mol-pl}} = \sum_{nl} (V_{nl} |e_n\rangle \langle g_n| C_l + V_{ln} |g_n\rangle \langle e_n| C_l^\dagger). \quad (3)$$

Here, the coupling coefficient reads $V_{nl} = d_{\text{mol}} d_{\text{pl}} \kappa_{nl} / R_n^3$. R_n denotes the distance between the center of the molecule n and that of the left lead, and \mathbf{n}_n is the related unit vector. The geometry factor takes the form $\kappa_{nl} = [\mathbf{e}_n \mathbf{e}_l] - 3 [\mathbf{e}_n \mathbf{n}_n] [\mathbf{n}_n \mathbf{e}_l]$. Although the coupling strength with higher plasmon modes may be larger than that with dipole plasmons, their corresponding energy transfer can be very weak if the molecules are off-resonant to them [17, 18]. This justifies the dipole-dipole interaction used here.

III. GENERAL APPROACH BASED ON REDUCED DENSITY MATRIX

In this section, we apply the open quantum system approach to investigate the dynamics of the molecular junction. The combined system of molecules and plasmon modes is described by the Hamiltonian $H_S = H_{\text{mol}} + H_{\text{pl}} + H_{\text{mol-pl}}$. The lead electron reservoirs influence the junction dynamics through incoherent processes between the neutral (ground and excited state) molecule and the ground negatively charged molecular state. Considering the reservoir Hamiltonian H_R and system-reservoir interaction H_{S-R} specified in [39, 40], we obtain a master equation for a density operator $\hat{\rho}$ (see below). We describe the system with a density matrix $\rho_{\alpha\mu, \beta\nu} \equiv \text{tr}_S \{ \hat{\rho} |\beta\nu\rangle \langle \alpha\mu| \}$. The matrix is constructed in a complete basis formed by the product states

$$|\alpha\mu\rangle = \prod_n |a_n\rangle \prod_l |\mu_l\rangle, \quad (4)$$

The index α abbreviates the set of molecular states $\{a_1, \dots, a_{N_m}\}$, and the index μ abbreviates the set of Fock state quantum numbers $\{\mu_x, \mu_y, \mu_z\}$. In our calculations, we include all the molecular states but truncate the plasmon multiple states at a maximum value.

A. Equation of Motion for Reduced Density Matrix

The equation of motion for $\hat{\rho}$ [18] reads

$$\frac{\partial}{\partial t} \hat{\rho} = -\frac{i}{\hbar} [H_S, \hat{\rho}] - \mathcal{D}[\hat{\rho}], \quad (5)$$

where the system Hamiltonian H_S was introduced in the previous section and the dissipative superoperator \mathcal{D} is chosen according to the following Lindblad-form

$$\mathcal{D}[\hat{\rho}] = \frac{1}{2} \sum_u k_u \left([\hat{L}_u^\dagger \hat{L}_u, \hat{\rho}]_+ - 2 \hat{L}_u \hat{\rho} \hat{L}_u^\dagger \right). \quad (6)$$

The plasmon damping with a total rate γ_{pl} is included by identifying \hat{L}_u as C_l and k_u as γ_{pl} . This rate is same for the three plasmon modes and includes both the interaction with radiation field and with electron-hole pair excitations inside the left lead. If the plasmon modes of the right lead are also relevant (not the case for the configuration in Fig.1(c)), we can also include their damping here.

Charging transitions into the charged molecular ground state may occur from both the ground and excited state of the neutral molecule. They are included in the treatment by choosing $\hat{L}_u = |f_n\rangle \langle b_n|$ and $k_u = k_{b \rightarrow f}^{(n)}$ with $b_n = g_n, e_n$. The charging rates $k_{b \rightarrow f}^{(n)}$ take the form

$$k_{b \rightarrow f}^{(n)} = \sum_X k_{Xb \rightarrow f}^{(n)} = \sum_X \Gamma_{Xbf}^{(n)} f_F(E_{fb}^{(n)} - \mu_X) \quad (7)$$

with the molecule-lead coupling function

$$\Gamma_{Xbf}^{(n)} = 2\pi \sum_{\mathbf{k}s} |V_{X\mathbf{k}s}^{nbf}|^2 \delta(\epsilon_{X\mathbf{k}} - E_{fb}^{(n)}) \quad (8)$$

multiplying the electron energy distribution f_F in the lead X . In the above expression, \mathbf{k} and s denote the wave-vector and spin of the electrons in the lead X . The coefficient $V_{X\mathbf{k}s}^{nbf}$ describes the amplitude of exchanging one electron between the lead $X = L, R$ and the molecule n , accompanying a molecular transition between the neutral state $|b_n\rangle$ and the singly charged state $|f_n\rangle$. The molecular charging is possible if the energy $\epsilon_{X\mathbf{k}}$ of electrons in the leads coincides with the charging energy $E_{fa}^{(n)} = E_{nf} - E_{na}$, cf. Eq. (8), which leads to the electron exchange scheme shown in Fig.1(c). The Fermi-distribution function f_F in Eq. (7) ascertains that only the occupied electron states in the leads contribute to the molecular charging. The lead chemical potentials assume the values $\mu_{X=L} = E_F + |e|V/2$ and $\mu_{X=R} = E_F - |e|V/2$ (for the case of a symmetrically applied voltage). Here, E_F is the chemical potential of the leads at zero-voltage bias, cf. the dashed line in Fig.1(c).

Discharge of the molecules towards the leads is similarly included by Lindblad terms with $\hat{L}_u = |b_n\rangle \langle f_n|$ and $k_u = k_{f \rightarrow b}^{(n)}$. The discharging rate is obtained from Eq. (7) by replacing f_F with $1 - f_F$ (only the unoccupied electron states in the leads are available for the molecular charge transfer).

Radiative decay of the excited molecular states, which is caused by interaction with quantized radiation field, can be also readily included in the equation (6). Since the molecular radiative decay rate is orders of magnitude weaker than the molecular charging and discharge rates [18], we are justified to ignore it in the present work.

B. Current Formula

The steady state current through the molecular junction is defined as the number of electrons passing through the molecules per time. This current can in turn be determined from the rate of the processes exchanging electrons between

the molecules and one of the leads (X):

$$I_X = \sum_{n=1}^{N_m} \sum_{b=g,e} \left(k_{Xb \rightarrow f}^{(n)} P_{nb} - k_{Xf \rightarrow b}^{(n)} P_{nf} \right), \quad (9)$$

where the charging and discharging rates, $k_{Xb \rightarrow f}^{(n)}$ and $k_{Xf \rightarrow b}^{(n)}$ were already introduced in the previous section, and P_{ng} , P_{ne} and P_{nf} are the populations of the neutral and the singly negatively charged molecular states $|g_n\rangle$, $|e_n\rangle$, and $|f_n\rangle$. The molecular populations are directly obtained from the solution of the master equation:

$$P_{nc} \equiv \text{tr}_S \{ \hat{\rho} |c_n\rangle \langle c_n| \} = \sum_{\mu} \sum_{\alpha'} \rho_{\alpha'\mu, \alpha'\mu}, \quad (10)$$

Here, the label $\alpha' = \{a_1, \dots, c_n, \dots, a_{N_m}\}$ indicates the molecular product states, where the molecule n is in the electronic state $|c_n\rangle = |g_n\rangle$, $|e_n\rangle$ or $|f_n\rangle$.

C. Emission Spectrum Formula

The master equation also gives access to the steady state power spectrum $F(\omega)$ of the emitted radiation. This quantity is evaluated as the Fourier transform of the two-time correlation function of the emitting dipoles,

$$F(\omega) = \frac{4\omega^3}{3\pi c^3 \hbar} \text{Re} \int_0^\infty dt e^{-i\omega t} \sum_{A,B} [\mathbf{d}_A \mathbf{d}_B^*] \langle \hat{X}_A^+(t) \hat{X}_B(0) \rangle. \quad (11)$$

The indices A and B indicate the contributions from the molecules and the plasmonic modes. Correspondingly, \hat{X}_A^+ and \hat{X}_B are transition operators $\hat{X}_A = |\varphi_{ng}\rangle \langle \varphi_{ne}|$, or $\hat{X}_A = C_I$, while \mathbf{d}_A and \mathbf{d}_B^* denote the corresponding transition dipole moments.

According to the quantum regression theorem [45], the two-time correlation functions defined by the expectation values $\langle \hat{X}_A^+(t) \hat{X}_B(0) \rangle \equiv \text{tr}_S \{ \hat{X}_A^+ \hat{\sigma}(B; t) \}$ can be calculated by propagating the operator (matrix) $\hat{\sigma}(B; t) \equiv \mathcal{U}(t) [\hat{X}_B \hat{\rho}_{ss}]$ with the same time-evolution super-operator $\mathcal{U}(t)$ that propagates the density matrix according to Eq. (5). The initial value for $\hat{\sigma}(B; t)$ is the product of the steady-state reduced density matrix $\hat{\rho}_{ss}$ and the matrix expression for \hat{X}_B ,

$$\begin{aligned} \sigma_{\alpha\mu, \beta\nu}(B, 0) &= \text{tr}_S \{ |\beta\nu\rangle \langle \alpha\mu| \hat{X}_B \hat{\rho}_{ss} \} \\ &= \sum_{\alpha'\mu'} \langle \alpha\mu | \hat{X}_B | \alpha'\mu' \rangle \rho_{\alpha'\mu', \beta\nu}^{(ss)}. \end{aligned} \quad (12)$$

Here, $\rho_{\alpha'\mu', \beta\nu}^{(ss)}$ is the reduced density matrix of the junction at steady-state.

The master equation solutions for $\rho_{\alpha\mu, \beta\nu}$ and $\sigma_{\alpha\mu, \beta\nu}(B, t)$ have been obtained for junctions with up to 5 molecules in [18]. There, it was demonstrated that with increasing number of molecules, higher plasmon excited states get populated and the emission becomes more narrowed. These results are similar to the lasing operation observed in experiments [3, 5, 13]. In fact, it is amplified spontaneous emission of plasmon rather than lasing since, on average, only about one quantum of plasmon is excited. To demonstrate lasing, we should

Table I. Physical parameters in our calculations (for further explanation see text)

$\hbar\omega_n$	2.6 eV	ΔE_{10}	1.3 eV
d_{mol}	16 D	$\hbar\Gamma_{\text{Ref}}^{(n)}$	50 meV
$\hbar\omega_{\text{pl}}$	2.6 eV	$\hbar\Gamma_{\text{Lgf}}^{(n)}$	30 meV
$\hbar\gamma_{\text{pl}}$	57 meV	$\hbar\Gamma_{\text{Lef}}^{(n)}, \hbar\Gamma_{\text{Rgf}}^{(n)}$	1 meV
d_{pl}	2925 D	V	3 V
$\Delta x_{\text{mol-MNP}}$	2.5 nm	$k_B T$	5 meV

consider junctions with more molecules. However, since the number $9^{N_m} (N_{\text{pl}} + 1)^2$ of $\rho_{\alpha\mu, \beta\nu}$ exponentially increases with N_m (N_{pl} indicates the highest excited plasmon state in the simulations), it is impossible to carry out the desired simulations. In the following sections we develop exact and approximate approaches that mitigate the nine-fold increase in computational effort for each extra molecule included in the system.

D. Parameters of Simulations

Here we specify the system parameters used in our simulations, see Table I. The left lead forms a spherical shape with 20 nm diameter, and the dipole plasmons have an excitation energy of $\hbar\omega_{\text{pl}} = 2.6$ eV, a transition dipole moment of $d_{\text{pl}} = 2925$ D, and a damping rate $\hbar\gamma_{\text{pl}} = 57$ meV [39]. The molecules are positioned at the left lead surface at a distance of $\Delta x_{\text{mol-MNP}} = 2.5$ nm. The molecular excitation energy shall be in complete resonance with the dipole plasmons, i.e., $\hbar\omega_n = 2.6$ eV. The molecular transition dipole moment is chosen as 16 D, which is in line with our previous study [18].

To specify the molecular charging and discharging rate, we introduce the so-called relative charged energy as $\Delta E_{10} = E_{nf} - E_{ng} - E_F$ (assumed to be identical for all the molecules, E_F is Fermi-energy at zero applied voltage bias) [37]. Here, we set it as $\Delta E_{10} = \hbar\omega_n/2$. The applied voltage is 3 V, at which the excited state of the neutral molecule is populated through electron transfer process [18]. The lead- and state-dependent molecule-lead couplings are chosen as $\hbar\Gamma_{\text{Ref}}^{(n)} = 50$ meV, $\hbar\Gamma_{\text{Lgf}}^{(n)} = 30$ meV and $\hbar\Gamma_{\text{Lef}}^{(n)} = \hbar\Gamma_{\text{Rgf}}^{(n)} = 1$ meV. As shown in [18], these values are optimal for the population inversion of the molecules and thus for the lead plasmon excitation. The thermal energy entering in the Fermi-distribution function is set as $k_B T = 5$ meV (at low temperature).

IV. APPROACH FOR JUNCTIONS WITH IDENTICAL MOLECULES

Next, a theoretical treatment of a junction with identical molecules is developed. In this case, the symmetry reduces the number of independent elements in the density matrix $\rho_{\alpha\mu, \beta\nu}$ because many matrix elements have identical values. The application of the symmetric effective parametrization to an ensemble of three-level system, as carried out here, gen-

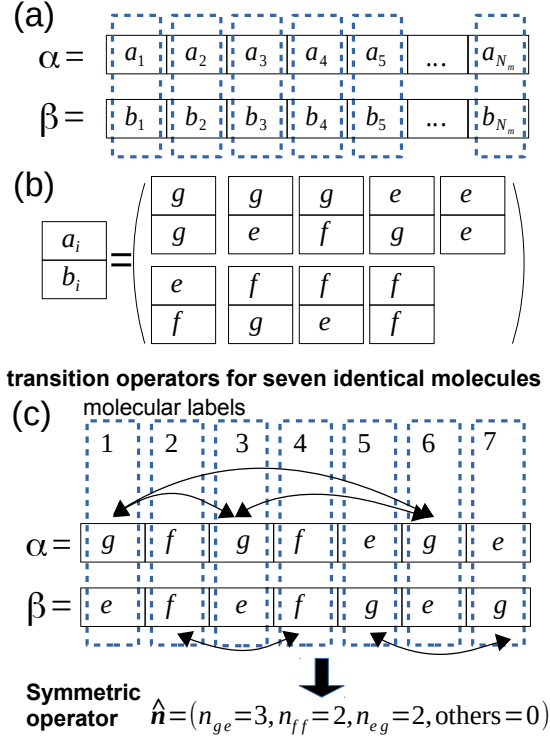


Figure 2. Transition operators $|\alpha\rangle\langle\beta|$ based on molecular product states $|\alpha\rangle, |\beta\rangle$ are mapped to vectors \mathbf{n} . Panel (a): expansion of the molecular product states. Panel (b): possible combinations (a_i, b_i) of quantum numbers related to individual molecules. Panel (c): some transition operators for seven identical molecules as one example; the group of molecules 1,3,6 is associated with the combination (g, e) , the group of molecules 2,4 with (f, f) , the group of molecules 5,7 with (e, g) ; the transition operators formed by exchanging the molecules in one group are identical; the set of those transition operators can be classified with the number of nine combinations in the panel (b) giving us a symmetric operator.

eralizes earlier work [17, 26] on the plasmonic nano-laser in which the emitters were modeled as two-level systems.

A. Symmetric Reduced Density Matrix

If all the molecules are identical, the original reduced density matrix (RDM) can be represented by a symmetric RDM according to the mapping $\rho_{\alpha\mu, \beta\nu} \equiv \text{tr}_S\{\hat{\rho}|\alpha\rangle\langle\beta| \times |\mu\rangle\langle\nu|\} \rightarrow \rho_{\mathbf{n}}^{\mu, \nu} \equiv \text{tr}_S\{\hat{\rho}\hat{n} \times |\mu\rangle\langle\nu|\}$. Here, the molecular transition operators $|\alpha\rangle\langle\beta|$ are mapped to symmetric operators \hat{n} , cf. Fig.2. The value of the symmetric operators is defined as $\mathbf{n} = (n_{gg}, n_{ge}, n_{gf}, n_{eg}, n_{ee}, n_{ef}, n_{fg}, n_{fe}, n_{ff})$ with nine positive integers in the range $[0, N_m]$, cf. Fig.2 (b). In general, these integers can be written as n_{cd} ($c, d = g, e, f$) and can be determined by the following formula $n_{cd} = \sum_{l=1}^{N_m} \delta_{a_l, c} \delta_{b_l, d}$, cf. Fig.2 (c) for systems with seven identical molecules. It indicates the number of molecules, which are on the state $|c\rangle$ in the product state $|\alpha\rangle$ and simultaneously on the state $|d\rangle$ in the product state $|\beta\rangle$. Here, a_l and b_l are elements of the sets

α and β , respectively. The above definition naturally leads to $\sum_{c,d} n_{cd} = N_m$. In fact, one symmetric RDM element represents a group of identical original RDM elements. Therefore, the treatment keeps all the information of systems without invoking any assumption. Because the above consideration is based on the product states rather than Dicke states, it can be readily applied for systems with multi-levels emitters [46].

We shall refer to the number of elements as the number of the vector \mathbf{n} . We consider N_m molecules as indistinguishable (identical) balls and the nine components of \mathbf{n} as nine distinguished boxes. Then, the number of \mathbf{n} is equal to the number of possibilities to put these balls into the boxes. The latter is a well-known combinatorial problem, and the result is $C_n^k \equiv n!/[k!(n-k)!]$ with $k+1$ boxes and $n+k$ balls. Therefore, the number of \mathbf{n} is $C_{N_m+8}^8$.

For the special configuration shown in Fig.1, only the plasmon mode $l = z$ interacts with the molecules. Therefore, the indices μ, ν in $\rho_{\alpha\mu, \beta\nu}$ and $\rho_{\mathbf{n}}^{\mu, \nu}$ are occupation numbers of the states $|\mu = \mu_z\rangle$ and $|\nu = \nu_z\rangle$. Due to the strong plasmon damping, very high laying plasmon states are expected to be unpopulated. Therefore, we can truncate the plasmon states in the simulations. We use N_{pl} to indicate the highest plasmon excited state considered. Consequently, the number of $\rho_{\mathbf{n}}^{\mu, \nu}$ is $n_{\text{tot}} = C_{N_m+8}^8 (N_{pl}+1)^2$. Notice that the number of $\rho_{\alpha\mu, \beta\nu}$ is $9^{N_m} (N_{pl}+1)^2$. Obviously, the size of $\rho_{\mathbf{n}}^{\mu, \nu}$ is much smaller than that of $\rho_{\alpha\mu, \beta\nu}$.

The equation of motion for $\rho_{\mathbf{n}}^{\mu, \nu}$ is obtained by replacing $\rho_{\alpha\mu, \beta\nu}$ in its equation with the corresponding $\rho_{\mathbf{n}}^{\mu, \nu}$ and noticing the definition of n_{cd} . The final result is

$$\begin{aligned} \frac{\partial}{\partial t} \rho_{\mathbf{n}}^{\mu, \nu} &= -i[(n_{eg} - n_{ge})\omega_{eg} + (n_{fg} - n_{gf})\omega_{fg} \\ &+ (n_{fe} - n_{ef})\omega_{fe}] \rho_{\mathbf{n}}^{\mu, \nu} - i\omega_{pl}(\mu - \nu) \rho_{\mathbf{n}}^{\mu, \nu} \\ &+ i\nu_{\text{mol-pl}} \sum_{a=g,e,f} [\sqrt{\nu} n_{ag} \rho_{(n_{ag}-1, n_{ae}+1)}^{\mu, \nu-1} \\ &- \sqrt{\mu+1} n_{ea} \rho_{(n_{ea}-1, n_{ga}+1)}^{\mu+1, \nu} + \sqrt{\nu+1} n_{ae} \rho_{(n_{ae}-1, n_{ag}+1)}^{\mu, \nu+1} \\ &- \sqrt{\mu} n_{ga} \rho_{(n_{ga}-1, n_{ea}+1)}^{\mu-1, \nu}] \\ &- (\gamma_{pl}/2) [(\mu + \nu) \rho_{\mathbf{n}}^{\mu, \nu} - 2\sqrt{(\nu+1)(\mu+1)} \rho_{\mathbf{n}}^{\mu+1, \nu+1}] \\ &- \sum_{b=g,e} (k_{b \rightarrow f}/2) [\sum_{a=g,e,f} (n_{ba} + n_{ab}) \rho_{\mathbf{n}}^{\mu, \nu} \\ &- 2n_{ff} \rho_{(n_{ff}-1, n_{bb}+1)}^{\mu, \nu}] \\ &- \sum_{b=g,e} (k_{f \rightarrow b}/2) [\sum_{a=g,e,f} (n_{fa} + n_{af}) \rho_{\mathbf{n}}^{\mu, \nu} \\ &- 2n_{bb} \rho_{(n_{bb}-1, n_{ff}+1)}^{\mu, \nu}]. \end{aligned} \quad (13)$$

Here, $\hbar\omega_{ab} = E_a - E_b$ are energy differences of molecular states. The coupling coefficient $\hbar\nu_{\text{mol-pl}} = V_{nl=z}$ is identical for all the molecules, cf. Eq.(3). $k_{b \rightarrow f} = k_{b \rightarrow f}^{(n)}$ and $k_{f \rightarrow b} = k_{f \rightarrow b}^{(n)}$ are molecular charging and discharge rate, respectively. If two components of \mathbf{n} change, we indicate the vec-

tors with these components, for example $(n_{gg} - 1, n_{ge} + 1) \equiv (n_{gg} - 1, n_{ge} + 1, n_{gf}, n_{eg}, n_{ee}, n_{ef}, n_{fg}, n_{fe}, n_{ff})$.

We can calculate the population of the product states $|\alpha\mu\rangle$ with the matrix elements $\rho_{\alpha\mu,\alpha\mu}$. According to the mapping, these elements correspond to $P_{(n_{gg},n_{ee},n_{ff})}^{\mu} \equiv \rho_{(n_{gg},0,0,0,n_{ee},0,0,0,n_{ff})}^{\mu,\mu}$. Here, n_{gg}, n_{ee}, n_{ff} are the number of molecules, which are in ground, excited and singly negatively charged state in the molecular product states $|\alpha\rangle$, respectively. The population of the states $|\alpha\rangle$ is given by $P_{(n_{gg},n_{ee},n_{ff})} = \sum_{\mu} P_{(n_{gg},n_{ee},n_{ff})}^{\mu}$. To calculate the population of the plasmon state $|\mu\rangle$, we should account for the fact that many $\rho_{\alpha\mu,\beta\nu}$ are mapped to one $\rho_n^{\mu,\nu}$. Finally, we get $P_{\mu} = \sum_{n_{gg}=0}^{N_m} \sum_{n_{ee}=0}^{N_m-n_{gg}} C_{N_m-1}^{n_{gg}-1} C_{N_m-n_{gg}}^{n_{ee}} P_{(n_{gg},n_{ee},N_m-n_{gg}-n_{ee})}^{\mu}$.

The current through the molecular junction can be calculated with the reformulated form of Eq. (9): $I_X = N_m \sum_{a=g,e} (k_{Xa \rightarrow f} P_a - k_{Xf \rightarrow a} P_f)$. The population $P_{nb} = P_b$ is identical for all the molecules with the values,

$$P_g = \sum_{n_{gg}=1}^{N_m} \sum_{n_{ee}=0}^{N_m-n_{gg}} C_{N_m-1}^{n_{gg}-1} C_{N_m-n_{gg}}^{n_{ee}} P_{(n_{gg},n_{ee},N_m-n_{gg}-n_{ee})}, \quad (14)$$

$$P_e = \sum_{n_{ee}=1}^{N_m} \sum_{n_{gg}=0}^{N_m-n_{ee}} C_{N_m-1}^{n_{ee}-1} C_{N_m-n_{ee}}^{n_{gg}} P_{(n_{gg},n_{ee},N_m-n_{gg}-n_{ee})}, \quad (15)$$

and

$$P_f = \sum_{n_{ff}=1}^{N_m} \sum_{n_{ee}=0}^{N_m-n_{ff}} C_{N_m-1}^{n_{ff}-1} C_{N_m-n_{ff}}^{n_{ee}} P_{(N_m-n_{ee}-n_{ff},n_{ee},n_{ff})}. \quad (16)$$

The emission formula given by Eq. (11) can be simplified as follows. Firstly, we notice, cf. Table I and [17], that the plasmon transition dipole moment \mathbf{d}_l is usually orders of magnitude larger than the molecular transition dipole moment \mathbf{d}_n and, hence, the contribution containing $[\mathbf{d}_l \mathbf{d}_l^*]$ dominates the emission formula. Secondly, only the plasmon mode $A = B = I = z$ contributes to the system emission (the index $B = z$ will be dropped in the following). Finally, we get the following expression

$$F(\omega) = \frac{4\omega^3 d_{pl}^2}{3\pi c^3 \hbar} \text{Re} \int_0^\infty dt e^{-i\omega t} \sum_{\mu} \sqrt{\mu} \sum_{n_{ff}=0}^{N_m} \sum_{n_{ee}=0}^{N_m-n_{ff}} C_{N_m}^{n_{ff}} C_{N_m-n_{ff}}^{n_{ee}} \times \sigma_{(N_m-n_{ff}-n_{ee},0,0,0,n_{ee},0,0,0,n_{ff})}^{\mu-1,\mu}(t). \quad (17)$$

The matrix $\sigma_n^{\mu,\nu}$ satisfies the same set of coupled equations (13) as $\rho_n^{\mu,\nu}$, with however the initial condition $\sigma_n^{\mu,\nu}(0) = \sqrt{\mu+1} \rho_n^{\mu+1,\nu}$ (ss) given by the steady state density matrix.

B. Effect due to Increasing Number of Molecules: Up to 10 Molecules

Simulations of junctions with up to $N_m = 5$ molecules were presented in [18]. Here, the equations (13) and (17) reduce

the computing time and allow calculations up to $N_m = 10$ molecules, where the number of matrix elements is reduced from around 3.5×10^{11} of $\rho_{\alpha\mu,\beta\nu}$ to around 4.3×10^6 of $\rho_n^{\mu,\nu}$.

The upper panel of Fig.3 shows the population of plasmon states. Generally speaking, the higher plasmon excited states are gradually populated when N_m increases, which indicates the compensation of plasmon damping and an increased plasmon excitation. The fourth and fifth excited plasmon states are populated for $N_m > 5$, which is in line with the prediction in [18]. The middle panel of Fig.3 shows the maximum and line-width of the related emission. The emission maximum increases from 0.1 for $N_m = 1$ to 1.2 for $N_m = 10$. The spectral line-width reduces from 25 meV for $N_m = 1$ to 14 meV for $N_m = 10$. The line narrowing can be explained by the Heisenberg's uncertainty principle [47]. Both of these observations we associate with the amplified spontaneous emission of the plasmon.

The lower panel of Fig.3 shows that the current through the junction (blue line) increases linearly with the number of molecules N_m . It increases from 1.68 μA for $N_m = 1$ to 23.54 μA for $N_m = 10$. The remaining lines indicate the population of molecular states, which are identical for all the molecules. The population of the neutral excited state P_e (red curve) decreases while the population of the neutral ground state P_g (black curve) and the charged state P_f (green curve) increase with increasing N_m and thus with increasing current through the junction.

It is expected in [17, 26] that when the system achieves lasing, the population of plasmon number states follows a Poisson-like distribution. Even with $N_m = 10$ emitters, we are only approaching the lasing threshold, and while $P_{\mu=1} \gtrsim P_{\mu=0}$, we do not yet see the characteristics of a Poisson distribution. Therefore, we can not claim the demonstration of lasing, but the calculations give reason to expect a Poisson-like distribution of plasmon state population for junctions with more molecules.

V. APPROXIMATE APPROACH BASED ON PLASMON REDUCED DENSITY MATRIX

In this section, an approximate approach motivated by the photon density matrix equation in the laser theory [42] is proposed for the molecular junction. A similar approach has been suggested in [17] to study the plasmonic nano-laser with a molecular optical pump. The idea is to derive an approximate equation for the plasmon mode by eliminating the molecular degrees of freedom. The computational effort by applying this approach is thus only limited by the highest excited plasmon state involved. Our derivation only assumes that all the molecules couple to one plasmon mode and although we will apply it to identical molecules it works also for junctions with different molecules.

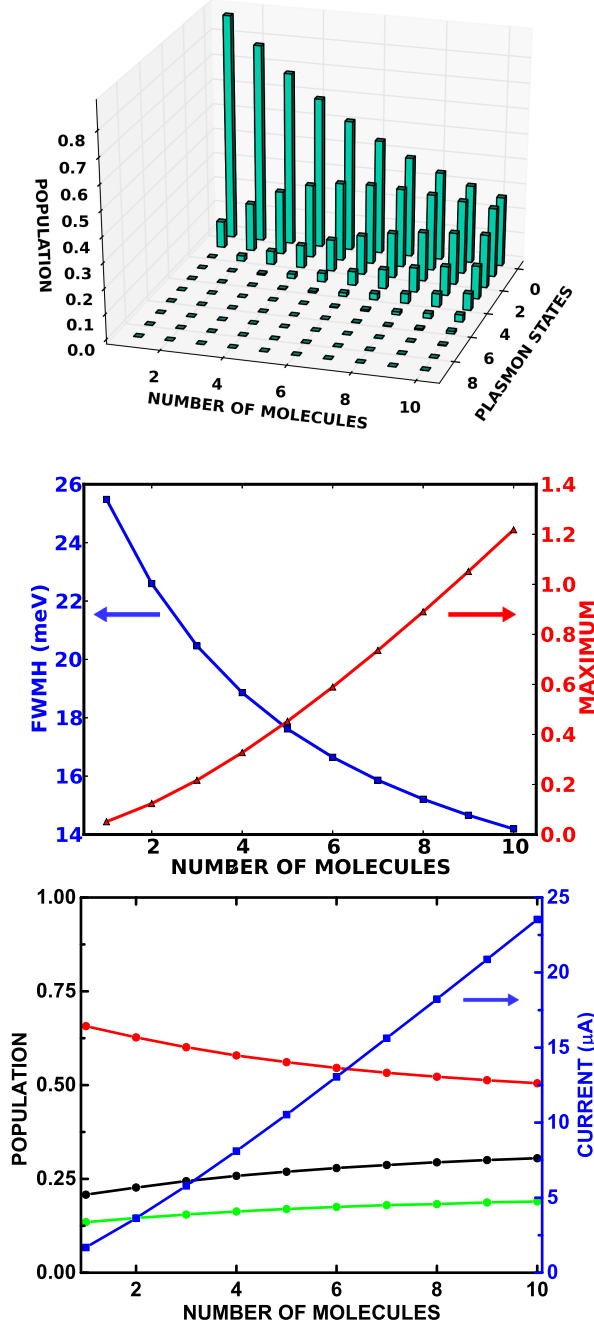


Figure 3. Steady-state properties of junctions with $N_m = 1 \dots 10$ molecules. Upper panel: population P_μ of excited plasmon states $|\mu\rangle$ for different N_m . Middle panel, properties of emission spectra for different N_m : blue curve with squares (left ordinate axis), emission line-width (FWHM); red curve with triangles (right ordinate axis), emission maximum. Lower panel: population of molecular states, red upper curve P_e , black middle curve P_g , and green lower curve P_f ; blue curve (right ordinate axis), current through the junctions. Other parameters according to Table I.

A. Approximate Equation of Motion for Plasmon Reduced Density Matrix

The plasmon reduced density matrix is defined by the expectation value: $\rho_{\mu\nu}(t) \equiv \text{tr}_S \{ \hat{\rho}(t) |v\rangle \langle \mu| \}$. The equation of motion for $\rho_{\mu\nu}$ can be obtained with Eq. (5):

$$\begin{aligned} \frac{\partial}{\partial t} \rho_{\mu\nu} = & -i\omega_{\mu\nu} \rho_{\mu\nu} - \gamma_{\text{pl}} [(\mu + \nu)/2] \rho_{\mu\nu} \\ & + \gamma_{\text{pl}} \sqrt{(\mu+1)(\nu+1)} \rho_{\mu+1\nu+1} \\ & - i \sum_{n=1}^{N_m} v_n (\sqrt{\mu+1} \rho_{g\mu+1, e\nu}^{(n)} + \sqrt{\mu} \rho_{e\mu-1, g\nu}^{(n)} \\ & - \sqrt{\nu} \rho_{g\mu, e\nu-1}^{(n)} - \sqrt{\nu+1} \rho_{e\mu, g\nu+1}^{(n)}). \end{aligned} \quad (18)$$

Here, $\hbar v_n$ is the coupling element between the plasmon and the molecule n and we have introduced $\omega_{\mu\nu} = (\mu - \nu) \omega_{\text{pl}}$. This equation depends on the expectation values of two operators: $\rho_{a\mu, b\nu}^{(n)} \equiv \text{tr}_S \{ \hat{\rho}(t) |b_n\rangle \langle a_n| \times |v\rangle \langle \mu| \}$, which describe the correlations of one molecule with the lead plasmon. The equations of motion for these correlations can be again derived with Eq. (5), cf. Appendix A. As demonstrated there, these equations depend on the expectation values of three operators, which describe the correlations of two molecules with the plasmon. Because of the dissipation the latter correlations are small and thus can be ignored in our treatment to obtain closed equations for $\rho_{\mu\nu}(t)$, see Eq. (A24).

The diagonal matrix element $\rho_{\mu\mu}$ is the population P_μ of the plasmon number state $|\mu\rangle$. From Eq. (A24) we obtain,

$$\begin{aligned} \frac{\partial}{\partial t} P_\mu = & (\gamma_{\text{pl}}(\mu+1) + k_{\mu+1}) P_{\mu+1} - p_\mu P_\mu \\ & - (\gamma_{\text{pl}}\mu + k_\mu) P_\mu + p_{\mu-1} P_{\mu-1}, \end{aligned} \quad (19)$$

The rates k_μ due to the coupling with the molecules reduce the population of higher plasmon excited states and increase the population of lower ones. In Eq. (19), the rate p_μ represents the molecule-induced excitation of the plasmon, which has opposite effect compared to k_μ . After some algebra, the molecule-induced plasmon damping and excitation rates can be written as

$$k_\mu = \sum_{n=1}^{N_m} k_\mu^{(n)} = \mu \sum_{n=1}^{N_m} \frac{2\kappa_\mu^{(n)} k_{e \rightarrow f}^{(n)} k_{f \rightarrow g}^{(n)} \Theta^{(n)} \bar{\Theta}^{(n)}}{1 + 2\kappa_\mu^{(n)} (\bar{\Theta}^{(n)} + \bar{\Xi}^{(n)}) \mu}, \quad (20)$$

$$p_{\mu-1} = \sum_{n=1}^{N_m} p_{\mu-1}^{(n)} = \mu \sum_{n=1}^{N_m} \frac{2\kappa_\mu^{(n)} k_{g \rightarrow f}^{(n)} k_{f \rightarrow e}^{(n)} \Xi^{(n)} \bar{\Xi}^{(n)}}{1 + 2\kappa_\mu^{(n)} (\bar{\Theta}^{(n)} + \bar{\Xi}^{(n)}) \mu}. \quad (21)$$

where $\Theta^{(n)} = \Theta_{\mu\mu}^{(n)}$, $\bar{\Theta}^{(n)} = \bar{\Theta}_{\mu\mu}^{(n)}$ as well as $\Xi^{(n)} = \Xi_{\mu\mu}^{(n)}$, $\bar{\Xi}^{(n)} = \bar{\Xi}_{\mu\mu}^{(n)}$. These quantities are defined in Eqs. (A15), (A16), (A17) and (A18), and do not depend on the plasmon quantum number μ . The plasmon state-dependent energy transfer rate is defined as

$$\kappa_\mu = \frac{v_n^2 (\delta_n + \delta_\mu)}{(\omega_n - \omega_{\text{pl}})^2 + (\delta_n + \delta_\mu)^2}. \quad (22)$$

Here, we have introduced the abbreviations: $\hbar\omega_n = E_{ne} - E_{ng}$, $\delta_n = (k_{g \rightarrow f}^{(n)} + k_{e \rightarrow f}^{(n)})/2$ as well as $\delta_\mu = \gamma_{pl} \left[(2\mu - 1)/2 - \sqrt{\mu(\mu - 1)} \right]$.

At steady-state, the time-derivative in Eq. (19) is zero, which leads to a linear algebraic equation for P_μ :

$$0 = (\gamma_{pl}(\mu + 1) + k_{\mu+1})P_{\mu+1} - p_\mu P_\mu - (\gamma_{pl}\mu + k_\mu)P_\mu + p_{\mu-1}P_{\mu-1}. \quad (23)$$

In the above equation, we get $(k_1\lambda_1 + \gamma_{pl})P_1 - p_0P_0 = 0$ by setting $\mu = 0$ (notice $k_0 = 0$ and $p_{-1} = 0$). Applying Eq. (23) repeatedly, we can easily get the following recursion relation

$$r_\mu = \frac{P_\mu}{P_{\mu-1}} = \frac{p_{\mu-1}}{\gamma_{pl}\mu + k_\mu}, \quad (24)$$

which together with normalization $\sum_\mu P_\mu = 1$ readily determines the population distribution of plasmon states. If the ratio r_μ is larger than unity for $\mu < \mu_c$ and smaller than unity for $\mu > \mu_c$, the plasmon state population will have a peak-like distribution around μ_c .

The current through the molecular junction can be evaluated with the following procedure (for more details, see Appendix B). According to Eq. (9) we should calculate the population of the molecular states $P_{nc} \equiv \text{tr}_S \{ \hat{\rho} |c_n\rangle \langle c_n| \} = \sum_\mu \rho_{c\mu, c\mu}^{(n)}$ to determine the current. Obviously, the population is related with the molecule-plasmon correlations $\rho_{c\mu, c\mu}^{(n)}$. These correlations have already been determined when we derive the approximate equation for the plasmon reduced density matrix $\rho_{\mu\nu}$. It is shown that they can be connected with $\rho_{\mu\nu}$ and therefore the current can be determined by $\rho_{\mu\nu}$. If the molecules are completely identical, the current becomes

$$\begin{aligned} I_X = & (k_{Xg \rightarrow f} + k_{Xf \rightarrow g} + k_{Xf \rightarrow e}) N_m k_{f \rightarrow g} k_{e \rightarrow f} \Theta \bar{\Theta} \\ & + (k_{Xe \rightarrow f} + k_{Xf \rightarrow g} + k_{Xf \rightarrow e}) N_m k_{f \rightarrow e} k_{g \rightarrow f} \Xi \bar{\Xi} \\ & - (k_{Xf \rightarrow g} + k_{Xf \rightarrow e}) N_m \\ & + (k_{Xg \rightarrow f} + k_{Xf \rightarrow g} + k_{Xf \rightarrow e}) \bar{\Theta} \gamma_{pl} \mathcal{N}_{pl} \\ & - (k_{Xe \rightarrow f} + k_{Xf \rightarrow g} + k_{Xf \rightarrow e}) \bar{\Xi} \gamma_{pl} \mathcal{N}_{pl}. \end{aligned} \quad (25)$$

The rates $k_{b \rightarrow f} = \sum_X k_{Xb \rightarrow f}^{(n)}$ and $k_{f \rightarrow b} = \sum_X k_{Xf \rightarrow b}^{(n)}$ ($b = g, e$) are the total charging and discharging rates while $k_{Xb \rightarrow f} = k_{Xb \rightarrow f}^{(n)}$ and $k_{Xf \rightarrow b} = k_{Xf \rightarrow b}^{(n)}$ are the parts related to the specific lead X , cf. Eq. (7). The above formula indicates that the current can be split into two parts. The first part is contributed by the first three lines in Eq. (25) and is proportional to the number of molecules. This part does not depend on the plasmon excitation. The second part is contributed by the remaining two lines in Eq. (25) and is proportional to the mean number of excited plasmons $\mathcal{N}_{pl} = \sum_\mu \mu P_\mu$.

B. Effect due to Increasing Number of Molecules: Up to 50 or more Molecules

We have verified the recursion relation, Eq. (24), (thus the approximate plasmon reduced density matrix) by using it to

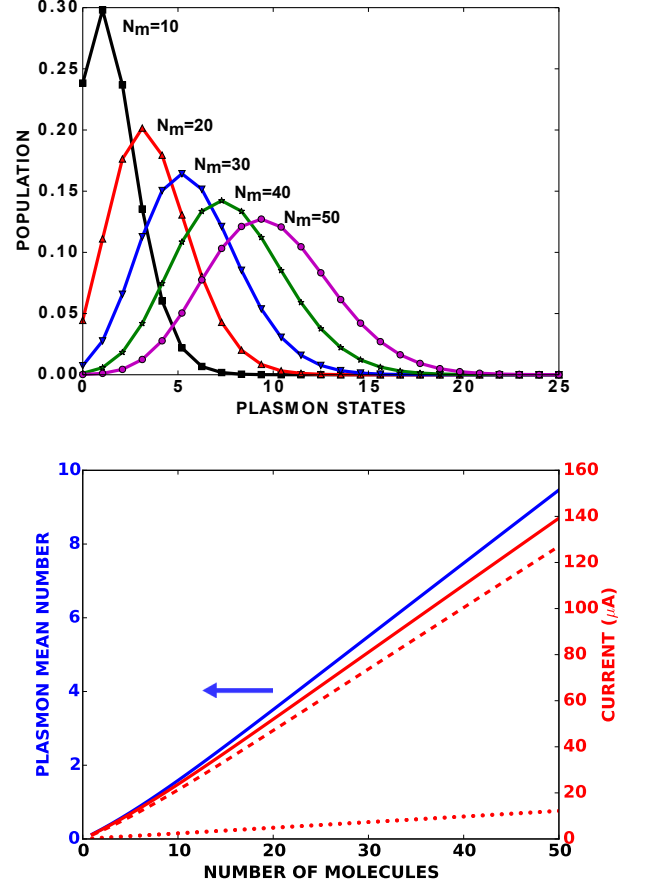


Figure 4. Steady-state properties of junctions with many molecules. Upper panel: plasmon state population for junctions with $N_m = 10, 20, 30, 40, 50$ molecules. Lower panel: blue solid curve (left ordinate axis), plasmon mean number \mathcal{N}_{pl} ; red upper solid curve, current $I = -I_L = I_R$ through the junctions; red middle dotted curve, current contribution proportional to N_m , cf. Eq.(25); red lower dashed curve, current contribution proportional to \mathcal{N}_{pl} , cf. Eq.(25). Other parameters according to Table I.

compute the plasmon state population for junctions with up to 10 molecules. The computation reproduces the exact numerical results, see the upper panel of Fig. 3. Then, we utilize the recursion relation to compute the plasmon state population for junctions with up to 50 molecules, see the upper panel of Fig.4. We see that the population distribution shifts to higher plasmon excited states when $N_m > 10$. When N_m increases from 20 to 50, the population distribution has a peak shape and the peak center is shifted from around $\mu = 3$ to around $\mu = 10$. In addition, the plasmon state populations approach the Poisson distribution, like the coherent state photon number distribution ascribed to the conventional laser.

We have also calculated the plasmon mean number \mathcal{N}_{pl} as well as the current through the junctions, cf. lower panel of Fig.3. There is almost no excitation for the junction with a single molecule ($\mathcal{N}_{pl} \approx 0$), while we obtain an average of nine plasmon quanta ($\mathcal{N}_{pl} = 9$) for the junction with $N_m = 50$ molecules. The current increases linearly from about $1.6 \mu A$

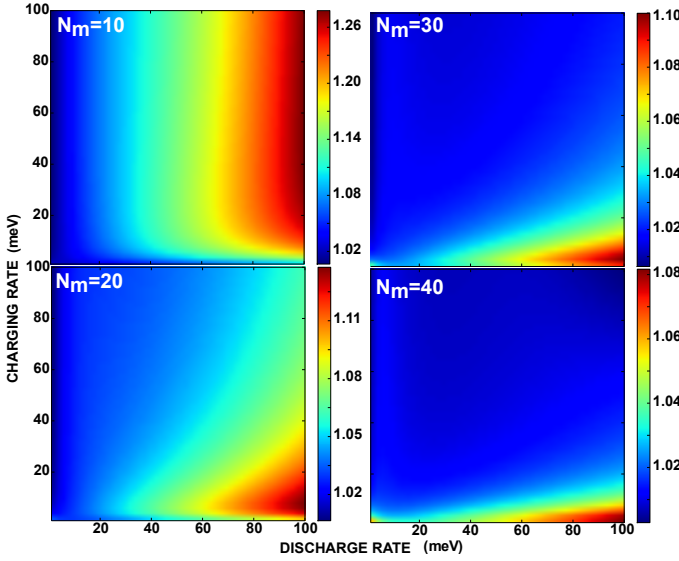


Figure 5. Second order equal-time intensity correlation function $g^{(2)}(0)$ for the emitted radiation as a function of the charging rate $\hbar k_{g \rightarrow f}^{(n)} = \hbar \Gamma_{Lgf}^{(n)}$ and discharging rate $\hbar k_{f \rightarrow e}^{(n)} = \hbar \Gamma_{Rfe}^{(n)}$ for different values of the number of molecules N_m . Other parameters are given in Table I.

for the junction with single molecule to $140 \mu\text{A}$ for the junction with $N_m = 50$ molecules (cf. red solid line). The equation (25) indicates that there are two contributions to the current. The terms explicitly depending on N_m are the contribution of the junctions in the absence of the lead plasmon, cf. the red dotted curve, which is due to electron transfer processes. The terms explicitly depending on \mathcal{N}_{pl} are the enhanced current due to the coupling with the lead plasmons, cf. the red dashed curve. It means extra energy is put into the system through the electron transfer process, which is in the end utilized to compensate the plasmon damping.

C. Intensity Correlation Function of Emitted Photons

The emitted photons from the nano-laser shows intensity fluctuations, characterized by the second-order intensity correlation function, which for equal times $g^{(2)}(0) = \langle a^+ a^+ a a \rangle / \langle a^+ a \rangle^2$, is given by a similar expression involving the plasmon mode operators, $g_{pl}^{(2)}(0) \equiv \langle C^+ C^+ C C \rangle / \langle C^+ C \rangle^2$. The value thus follows directly from the steady state excitation number distribution calculated above. Photon bunching ($g^{(2)}(0) > 1$), is equivalent to a super Poisson plasmon number distribution with $\text{Var}(\mu) > \mathcal{N}_{pl} = \sum_{\mu} \mu P_{\mu}$.

In Fig.5, the $g_{pl}^{(2)}(0)$ function of junctions with 10, 20, 30 and 40 molecules is shown for different charging $k_{g \rightarrow f}^{(n)} = \Gamma_{Lgf}^{(n)}$ and discharging rates $k_{f \rightarrow e}^{(n)} = \Gamma_{Rfe}^{(n)}$. $g_{pl}^{(2)}(0)$ is always larger than unity, implying that the emitted photons are bunched and the plasmon number distribution is super-Poisson. For a fixed charging rate $k_{g \rightarrow f}^{(n)}$, the bunching increases with increasing

discharging rate $k_{f \rightarrow e}^{(n)}$. For a fixed $k_{f \rightarrow e}^{(n)}$ it approaches a constant with increasing charging rate $k_{g \rightarrow f}^{(n)}$ for the junction with 10 molecules, while junctions with more than 20 molecules show a decrease towards $g_{pl}^{(2)}(0) = 1$ with increasing charging rate $k_{g \rightarrow f}^{(n)}$, reflecting the approach to Poisson statistics characteristic of lasing.

VI. APPROXIMATE APPROACH BASED ON NONLINEAR RATE EQUATIONS

In our previous study [18] we have derived rate equations for the molecular state population and plasmon mean number for a junction with a single molecule. Here, we extend these equations to junctions with many molecules.

Our starting point is the equations for the population of the molecular states $P_{na} \equiv \text{tr}_S \{ \hat{\rho}(t) |a_n\rangle \langle a_n| \}$ (more details see Appendix C). The equations for P_{ne} and P_{ng} depend on the molecule-plasmon correlations of the type $\langle |g_n\rangle \langle e_n| C^+ \rangle \equiv \text{tr}_S \{ \hat{\rho}(t) |g_n\rangle \langle e_n| C^+ \}$. These correlations decay much faster than the molecular state populations because of the plasmon dissipation, and thus we assume that they adiabatically follow the populations P_{na} . Inserting the adiabatic solutions of the correlations back into the equations for P_{na} , we get

$$\frac{\partial}{\partial t} P_{nf} = - \left(k_{f \rightarrow g}^{(n)} + k_{f \rightarrow e}^{(n)} \right) P_{nf} + k_{e \rightarrow f}^{(n)} P_{ne} + k_{g \rightarrow f}^{(n)} P_{ng}, \quad (26)$$

$$\frac{\partial}{\partial t} P_{ne} = -k_{e \rightarrow f}^{(n)} P_{ne} + k_{f \rightarrow e}^{(n)} P_{nf} + \kappa_n \mathcal{N}_{pl} P_{ng} - \kappa_n [1 + \mathcal{N}_{pl}] P_{ne}, \quad (27)$$

$$\frac{\partial}{\partial t} P_{ng} = -k_{g \rightarrow f}^{(n)} P_{ng} + k_{f \rightarrow g}^{(n)} P_{nf} - \kappa_n \mathcal{N}_{pl} P_{ng} + \kappa_n [1 + \mathcal{N}_{pl}] P_{ne}. \quad (28)$$

Here, the energy transfer rates are defined as $\kappa_n = 2\nu_n^2 \gamma_n / [(\omega_{pl} - \omega_n)^2 + \gamma_n^2]$ with $\gamma_n = (\gamma_{pl} + k_{e \rightarrow f}^{(n)} + k_{g \rightarrow f}^{(n)})/2$. Notice the above equations depend on the plasmon mean number $\mathcal{N}_{pl} \equiv \langle C^+ C \rangle$. The equation for \mathcal{N}_{pl} also depends on the molecule-plasmon correlations. With the adiabatic solution for the correlations, we can get the following equation

$$\frac{\partial}{\partial t} \mathcal{N}_{pl} = \sum_{n=1}^{N_m} \kappa_n (P_{ne} + \mathcal{N}_{pl} (P_{ne} - P_{ng})) - \gamma_{pl} \mathcal{N}_{pl}, \quad (29)$$

where $\kappa_n P_{ne}$, $\kappa_n \mathcal{N}_{pl} P_{ne}$ and $-\kappa_n \mathcal{N}_{pl} P_{ng}$ represent spontaneous and stimulated emission, as well as stimulated absorption of plasmon excitation by the molecules.

A. Comparison of the Plasmon Mean Number Calculated with Different Approaches

In Fig.6, we compare the different approaches for the calculation of the plasmon mean number for junctions with different numbers of molecules. These approaches are based on the full reduced density matrix (RDM) equation (black stars),

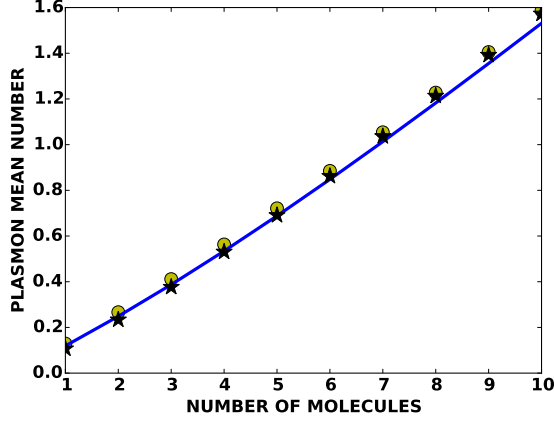


Figure 6. Plasmon mean number calculated with different approaches for junctions with different numbers of molecules N_m . Black stars: calculations based on simplified reduced density matrix equation Eq.(13). Yellow circles: calculations based on recursion relation Eq.(24). Blue solid line: calculations based on rate equations (26),(27),(28) and (29). Other parameters according to Table I.

the population recursion relation (derived from the plasmon RDM, yellow circles) as well as the rate equations (blue solid line). The plasmon mean number increases almost linearly with increasing number of molecules. The green squares approach the black dots from above when the number of molecules in the junction increases and this proves the validity of the plasmon RDM in that limit. We have also compared the results of the plasmon RDM with the results of the rate equations for junctions with up to 50 molecules and found that the latter slightly underestimate the plasmon mean number (not shown). We explain this by the overestimation of the spontaneous energy transfer, cf. the discussion about Fig. 7 in [17].

VII. CONCLUSIONS

We have extended the study [18] of the electroluminescence of a molecular junction excited through an energy exchange coupling with electron-transfer induced excited molecules to the junctions with many molecules. In the present article, we simplified the full system master equation by utilizing symmetries of the density matrix for identical molecules. We carried out exact simulations for junctions with up to 10 molecules. With increasing number of molecules, higher excited states of the lead plasmon are populated, accompanied by a narrowing of the emission, indicating the amplified emission of the plasmon.

Our analysis did not incorporate the coherence induced by the excitonic and charge transfer coupling among the molecules. The excitonic coupling between molecules can in principle be introduced in the system Hamiltonian, while the charge transfer coupling may be treated as incoherent terms in the RDM equations. These couplings become important if the molecular ensemble is dense and constitute an interesting topic for further studies.

Approximate equations of motion for the plasmon degrees of freedom were derived, and for junctions in steady-state, a recursion relation was obtained for the plasmon state populations. The population distribution of the plasmon states is Poisson-like, and the intensity fluctuations of the emitted radiation are reduced for junctions with more than 20 molecules, which indicates the formation of a plasmon coherent state. Finally, non-linear rate equations were derived for the molecular state populations and the average plasmon excitation, which well account for the main features found by the other methods.

Thus validated, the symmetric approaches may also be applied to junctions with many different molecules and to junctions, where the molecules couple to several plasmon modes. Our analysis is carried out for a particular pumping mechanism involving electron transfer to excited molecular states, but the approaches outlined may find wider application for other systems with similar excitation mechanisms, for example, the optically pumped nano-laser [46] and the semiconductor-based plasmonic nano-laser [13, 14].

ACKNOWLEDGMENTS

Y.Z. acknowledges Yaroslav Zelinskyy, Dirk Ziemann and Thomas Plehn for several illuminating discussions. This work was supported by the *Deutsche Forschungsgemeinschaft* through Sfb 951 and by the GIF research Grant No. 1146-73.14/2011 (V. M.), by the *China Scholarship Council* (Y. Z.), as well as the Villum Foundation (Y. Z. and K. M.).

Appendix A: Derivation of the Approximate Plasmon Reduced Density Matrix Equation

The equations for the molecule-plasmon correlations $\rho_{a\mu,b\nu}^{(n)}$ can be written as

$$\begin{aligned} & \frac{\partial}{\partial t} \rho_{g\mu,g\nu}^{(n)} \\ &= -i\omega_{\mu\nu} \rho_{g\mu,g\nu}^{(n)} - k_{g \rightarrow f}^{(n)} \rho_{g\mu,g\nu}^{(n)} + k_{f \rightarrow g}^{(n)} \rho_{f\mu,f\nu}^{(n)} \\ & - \gamma_{pl} [(\mu + \nu)/2] \rho_{g\mu,g\nu}^{(n)} + \gamma_{pl} \sqrt{(\mu + 1)(\nu + 1)} \rho_{g\mu+1,g\nu+1}^{(n)} \\ & + i\nu_n \left(\sqrt{\nu} \rho_{g\mu,e\nu-1}^{(n)} - \sqrt{\mu} \rho_{e\mu-1,g\nu}^{(n)} \right), \end{aligned} \quad (A1)$$

$$\begin{aligned} & \frac{\partial}{\partial t} \rho_{g\mu,e\nu-1}^{(n)} \\ &= i(\tilde{\omega}_n^* - \omega_{\mu\nu-1}) \rho_{g\mu,e\nu-1}^{(n)} \\ & - \gamma_{pl} [(\mu + \nu - 1)/2] \rho_{g\mu,e\nu-1}^{(n)} + \gamma_{pl} \sqrt{(\mu + 1)\nu} \rho_{g\mu+1,e\nu}^{(n)} \\ & + i\nu_n \left(\sqrt{\nu} \rho_{g\mu,g\nu}^{(n)} - \sqrt{\mu} \rho_{e\mu-1,e\nu-1}^{(n)} \right), \end{aligned} \quad (A2)$$

$$\begin{aligned}
& \frac{\partial}{\partial t} \rho_{e\mu-1,gv}^{(n)} \\
&= -i(\tilde{\omega}_n + \omega_{\mu-1\nu}) \rho_{e\mu-1,gv}^{(n)} \\
&- \gamma_{pl} [(\mu-1+\nu)/2] \rho_{e\mu-1,gv}^{(n)} + \gamma_{pl} \sqrt{\mu(\nu+1)} \rho_{e\mu,gv+1}^{(n)} \\
&+ i\nu_n \left(\sqrt{\nu} \rho_{e\mu-1,gv-1}^{(n)} - \sqrt{\mu} \rho_{g\mu,gv}^{(n)} \right), \quad (A3)
\end{aligned}$$

$$\begin{aligned}
& \frac{\partial}{\partial t} \rho_{e\mu-1,gv-1}^{(n)} \\
&= -i\omega_{\mu-1\nu-1} \rho_{e\mu-1,gv-1}^{(n)} - k_{e\rightarrow f}^{(n)} \rho_{e\mu-1,gv-1}^{(n)} + k_{f\rightarrow e}^{(n)} \rho_{f\mu-1,gv-1}^{(n)} \\
&- \gamma_{pl} [(\mu+\nu-2)/2] \rho_{e\mu-1,gv-1}^{(n)} + \gamma_{pl} \sqrt{\mu\nu} \rho_{e\mu,gv}^{(n)} \\
&+ i\nu_n \left(\sqrt{\nu} \rho_{e\mu-1,gv}^{(n)} - \sqrt{\mu} \rho_{g\mu,gv-1}^{(n)} \right), \quad (A4)
\end{aligned}$$

$$\begin{aligned}
& \frac{\partial}{\partial t} \rho_{f\mu,f\nu}^{(n)} \\
&= -i\omega_{\mu\nu} \rho_{f\mu,f\nu}^{(n)} + k_{g\rightarrow f}^{(n)} \rho_{g\mu,gv}^{(n)} + k_{e\rightarrow f}^{(n)} \rho_{e\mu,gv}^{(n)} \\
&- \gamma_{pl} [(\mu+\nu)/2] \rho_{f\mu-1,f\nu-1}^{(n)} + \gamma_{pl} \sqrt{(\mu+1)(\nu+1)} \rho_{f\mu,f\nu}^{(n)} \\
&- \left(k_{f\rightarrow g}^{(n)} + k_{f\rightarrow e}^{(n)} \right) \rho_{f\mu,f\nu}^{(n)}. \quad (A5)
\end{aligned}$$

Here, we have introduced the complex transition frequencies $\tilde{\omega}_n = \omega_n - i\delta_n$ with $\delta_n = (k_{g\rightarrow f}^{(n)} + k_{e\rightarrow f}^{(n)})/2$. The above equations actually also depend on the correlations $\rho_{ab\mu,cd\nu}^{(n,n')} \equiv \text{tr}_s \{ \hat{\rho}(t) |c_n\rangle \langle a_n| \times |d_{n'}\rangle \langle b_{n'}| \times |\nu\rangle \langle \mu| \}$ ($n \neq n'$) of two different molecules and the plasmon mode. These coherences decay faster than the single molecule-plasmon correlations $\rho_{a\mu,b\nu}^{(n)}$, and therefore are neglected in our approximate treatment. Next, we assume a moderate variation of density matrix elements with the plasmon number and replace the term $\sqrt{(\mu+1)(\nu+1)} \rho_{a\mu+1,b\nu+1}^{(n)}$ by $\sqrt{\mu\nu} \rho_{a\mu,b\nu}^{(n)}$, and write

$$\begin{aligned}
& -[i\omega_{\mu\nu} - \gamma_{pl}(\mu+\nu)/2] \rho_{a\mu,b\nu}^{(n)} \\
&+ \gamma_{pl} \sqrt{(\mu+1)(\nu+1)} \rho_{a\mu+1,b\nu+1}^{(n)} \rightarrow -i\tilde{\omega}_{\mu\nu} \rho_{a\mu,b\nu}^{(n)}, \quad (A6)
\end{aligned}$$

where we have introduced the complex frequency $\tilde{\omega}_{\mu\nu} = \omega_{\mu\nu} - i\gamma_{pl}[(\mu+\nu)/2 - \sqrt{\mu\nu}]$.

To proceed we notice that only the dissipation of the plasmon contributes to the equation (18) for $\rho_{\mu\nu}$. In contrast, the dissipation of both the molecule and the plasmon contributes to the equations for $\rho_{a\mu,b\nu}^{(n)}$. This implies that $\rho_{a\mu,b\nu}^{(n)}$ change much faster and thus may *adiabatically* follow the change of $\rho_{\mu\nu}$. The approximate version of the equations (A1) to (A5) do not explicitly depend on $\rho_{\mu\nu}$. However, due to the relation $\rho_{f\mu,f\nu}^{(n)} + \rho_{e\mu,gv}^{(n)} + \rho_{g\mu,gv}^{(n)} = \rho_{\mu\nu}$, they actually implicitly couple with the equation (18) for $\rho_{\mu\nu}$. From Eq. (A5), we express $\rho_{f\mu,f\nu}^{(n)}$ with $\rho_{e\mu,gv}^{(n)}$ by replacing $\rho_{g\mu,gv}^{(n)}$ with $\rho_{\mu,\nu} - \rho_{f\mu,f\nu}^{(n)} - \rho_{e\mu,gv}^{(n)}$. Similarly, we can also express $\rho_{f\mu,f\nu}^{(n)}$ with $\rho_{g\mu,gv}^{(n)}$ by replacing $\rho_{e\mu,gv}^{(n)}$ with $\rho_{\mu,\nu} - \rho_{f\mu,f\nu}^{(n)} - \rho_{g\mu,gv}^{(n)}$. Then, we insert the results to Eqs. (A2) and (A3) and get

$$\begin{aligned}
\rho_{g\mu,gv-1}^{(n)} &= \lambda_{\mu\nu}^{(n)} \left(a_{\mu\nu}^{(n)} \sqrt{\mu} + c_{\mu\nu}^{(n)} \sqrt{\nu} \right) g_{\mu-1\nu-1}^{(n)} \rho_{\mu-1\nu-1} \\
&- \lambda_{\mu\nu}^{(n)} \left(a_{\mu\nu}^{(n)} \sqrt{\nu} + c_{\mu\nu}^{(n)} \sqrt{\mu} \right) f_{\mu\nu}^{(n)} \rho_{\mu\nu}, \quad (A7)
\end{aligned}$$

$$\begin{aligned}
\rho_{e\mu-1,gv}^{(n)} &= \lambda_{\mu\nu}^{(n)} \left(b_{\mu\nu}^{(n)} \sqrt{\nu} - c_{\mu\nu}^{(n)} \sqrt{\mu} \right) g_{\mu-1\nu-1}^{(n)} \rho_{\mu-1\nu-1} \\
&- \lambda_{\mu\nu}^{(n)} \left(b_{\mu\nu}^{(n)} \sqrt{\mu} - c_{\mu\nu}^{(n)} \sqrt{\nu} \right) f_{\mu\nu}^{(n)} \rho_{\mu\nu}. \quad (A8)
\end{aligned}$$

In the above expressions, we have introduced the following abbreviations

$$a_{\mu\nu}^{(n)} = (\tilde{\omega}_n + \tilde{\omega}_{\mu-1\nu}) - i\nu_n^2 \left(\tilde{\Xi}_{\mu-1\nu-1}^{(n)} \nu + \tilde{\Theta}_{\mu\nu}^{(n)} \mu \right), \quad (A9)$$

$$b_{\mu\nu}^{(n)} = (\tilde{\omega}_n^* - \tilde{\omega}_{\mu\nu-1}) + i\nu_n^2 \left(\tilde{\Theta}_{\mu\nu}^{(n)} \nu + \tilde{\Xi}_{\mu-1\nu-1}^{(n)} \mu \right), \quad (A10)$$

$$c_{\mu\nu}^{(n)} = i\nu_n^2 \left(\tilde{\Theta}_{\mu\nu}^{(n)} + \tilde{\Xi}_{\mu-1\nu-1}^{(n)} \right) \sqrt{\mu\nu}, \quad (A11)$$

$$f_{\mu\nu}^{(n)} = \nu_n k_{f\rightarrow g}^{(n)} k_{e\rightarrow f}^{(n)} \tilde{\Theta}_{\mu\nu}^{(n)} \tilde{\Theta}_{\mu\nu}^{(n)}, \quad (A12)$$

$$g_{\mu\nu}^{(n)} = \nu_n k_{f\rightarrow e}^{(n)} k_{g\rightarrow f}^{(n)} \tilde{\Xi}_{\mu\nu}^{(n)} \tilde{\Xi}_{\mu\nu}^{(n)}, \quad (A13)$$

as well as

$$1/\lambda_{\mu\nu}^{(n)} = a_{\mu\nu}^{(n)} b_{\mu\nu}^{(n)} + c_{\mu\nu}^{(n)} c_{\mu\nu}^{(n)}. \quad (A14)$$

In addition, the following abbreviations have been used:

$$1/\Theta_{\mu\nu}^{(n)} = i\tilde{\omega}_{\mu\nu} + k_{f\rightarrow g}^{(n)} + k_{f\rightarrow e}^{(n)} + k_{e\rightarrow f}^{(n)}, \quad (A15)$$

$$1/\Xi_{\mu\nu}^{(n)} = i\tilde{\omega}_{\mu\nu} + k_{f\rightarrow g}^{(n)} + k_{f\rightarrow e}^{(n)} + k_{g\rightarrow f}^{(n)}, \quad (A16)$$

$$1/\tilde{\Theta}_{\mu\nu}^{(n)} = i\tilde{\omega}_{\mu\nu} + k_{g\rightarrow f}^{(n)} - k_{f\rightarrow g}^{(n)} \left(k_{g\rightarrow f}^{(n)} - k_{e\rightarrow f}^{(n)} \right) \tilde{\Theta}_{\mu\nu}^{(n)}, \quad (A17)$$

$$1/\tilde{\Xi}_{\mu\nu}^{(n)} = i\tilde{\omega}_{\mu\nu} + k_{e\rightarrow f}^{(n)} - k_{f\rightarrow e}^{(n)} \left(k_{e\rightarrow f}^{(n)} - k_{g\rightarrow f}^{(n)} \right) \tilde{\Xi}_{\mu\nu}^{(n)}, \quad (A18)$$

The solutions for $\rho_{g\mu,gv}^{(n)}$ and $\rho_{e\mu-1,gv-1}^{(n)}$ are

$$\begin{aligned}
\rho_{g\mu,gv}^{(n)} &= i\nu_n \tilde{\Theta}_{\mu\nu}^{(n)} (i_{\mu\nu}^{(n)} \rho_{\mu\nu} - h_{\mu\nu}^{(n)} g_{\mu-1\nu-1}^{(n)} \rho_{\mu-1\nu-1}) \\
&+ k_{f\rightarrow g}^{(n)} k_{e\rightarrow f}^{(n)} \tilde{\Theta}_{\mu\nu}^{(n)} \tilde{\Theta}_{\mu\nu}^{(n)} \rho_{\mu\nu}, \quad (A19)
\end{aligned}$$

$$\begin{aligned}
\rho_{e\mu-1,gv-1}^{(n)} &= i\nu_n \tilde{\Xi}_{\mu-1\nu-1}^{(n)} (j_{\mu\nu}^{(n)} g_{\mu-1\nu-1}^{(n)} \rho_{\mu-1\nu-1} - h_{\mu\nu}^{(n)} f_{\mu\nu}^{(n)} \rho_{\mu\nu}) \\
&+ k_{f\rightarrow e}^{(n)} k_{g\rightarrow f}^{(n)} \tilde{\Xi}_{\mu-1\nu-1}^{(n)} \tilde{\Xi}_{\mu-1\nu-1}^{(n)} \rho_{\mu-1\nu-1}, \quad (A20)
\end{aligned}$$

where we have introduced the following abbreviations:

$$h_{\mu\nu}^{(n)} = \lambda_{\mu\nu}^{(n)} \left[\left(b_{\mu\nu}^{(n)} - a_{\mu\nu}^{(n)} \right) \sqrt{\mu\nu} - c_{\mu\nu}^{(n)} (\mu + \nu) \right], \quad (A21)$$

$$i_{\mu\nu}^{(n)} = \lambda_{\mu\nu}^{(n)} \left(b_{\mu\nu}^{(n)} \mu - a_{\mu\nu}^{(n)} \nu - 2c_{\mu\nu}^{(n)} \sqrt{\mu\nu} \right), \quad (A22)$$

$$j_{\mu\nu}^{(n)} = \lambda_{\mu\nu}^{(n)} \left(b_{\mu\nu}^{(n)} \nu - a_{\mu\nu}^{(n)} \mu - 2c_{\mu\nu}^{(n)} \sqrt{\mu\nu} \right). \quad (A23)$$

Inserting Eqs. (A7) and (A8) into Eq. (18), we finally get the master equation for the plasmon reduced density matrix

$$\begin{aligned} \frac{\partial}{\partial t} \rho_{\mu\nu} = & -i\omega_{\mu\nu} \rho_{\mu\nu} - \gamma_{\text{pl}} [(\mu + \nu)/2] \rho_{\mu\nu} \\ & + \gamma_{\text{pl}} \sqrt{(\mu + 1)(\nu + 1)} \rho_{\mu+1\nu+1} \\ & - i \sum_n v_n (h_{\mu+1\nu+1}^{(n)} f_{\mu+1\nu+1}^{(n)} \rho_{\mu+1\nu+1} \\ & + h_{\mu\nu}^{(n)} g_{\mu-1\nu-1}^{(n)} \rho_{\mu-1\nu-1} \\ & - j_{\mu+1\nu+1}^{(n)} g_{\mu\nu}^{(n)} \rho_{\mu\nu} - i_{\mu\nu}^{(n)} f_{\mu\nu}^{(n)} \rho_{\mu\nu}). \end{aligned} \quad (\text{A24})$$

The equation for the populations $\rho_{\mu\mu}$ is given by Eq. (19) in the main text. In that equation, the rates induced by the molecules are defined as $k_\mu \equiv -i \sum_n v_n h_{\mu\mu}^{(n)} f_{\mu\mu}^{(n)}$ and $p_\mu \equiv -i \sum_n v_n h_{\mu+1\mu+1}^{(n)} g_{\mu\mu}^{(n)}$.

Appendix B: Current Through the Molecular Junction

The current through the molecular junction is calculated with the formula (9). That formula depends on the populations of molecular levels $P_{nb} \equiv \text{tr} \{ \hat{\rho} |b_n\rangle \langle b_n| \} = \sum_\mu \rho_{b\mu, b\mu}^{(n)}$. From Eqs. (A19) and (A20), we directly get the expressions for the molecule-plasmon correlations $\rho_{g\mu, g\mu}^{(n)}$ and $\rho_{e\mu, e\mu}^{(n)}$:

$$\begin{aligned} \rho_{g\mu, g\mu}^{(n)} = & \bar{\Theta}^{(n)} \left(p_{\mu-1}^{(n)} P_{\mu-1} - k_\mu^{(n)} P_\mu \right) \\ & + k_{f \rightarrow g}^{(n)} k_{e \rightarrow f}^{(n)} \bar{\Theta}^{(n)} \bar{\Theta}^{(n)} P_\mu, \end{aligned} \quad (\text{B1})$$

$$\begin{aligned} \rho_{e\mu-1, e\mu-1}^{(n)} = & \bar{\Xi}^{(n)} \left(k_\mu^{(n)} P_\mu - p_{\mu-1}^{(n)} P_{\mu-1} \right) \\ & + k_{f \rightarrow e}^{(n)} k_{g \rightarrow f}^{(n)} \bar{\Xi}^{(n)} \bar{\Xi}^{(n)} P_{\mu-1}, \end{aligned} \quad (\text{B2})$$

where $k_\mu^{(n)}$ and $p_{\mu-1}^{(n)}$ are defined in Eqs. (20) and (21). Notice that $\bar{\Theta}^{(n)} \equiv \bar{\Theta}_{\mu\mu}^{(n)}$, $\bar{\Theta}^{(n)} \equiv \bar{\Theta}_{\mu\mu}^{(n)}$ and $\bar{\Xi}^{(n)} \equiv \bar{\Xi}_{\mu\mu}^{(n)}$, $\bar{\Xi}^{(n)} \equiv \bar{\Xi}_{\mu\mu}^{(n)}$ do not depend on μ . The remaining molecule-plasmon correlation $\rho_{f\mu, f\mu}^{(n)}$ can be calculated with the relation $\rho_{f\mu, f\mu}^{(n)} = P_\mu - \rho_{g\mu, g\mu}^{(n)} - \rho_{e\mu, e\mu}^{(n)}$.

If all the molecules are identical, Eq. (9) can be reformulated as

$$I_X = N_m \sum_{a=g,e} (k_{Xa \rightarrow f} P_a - k_{Xf \rightarrow a} P_f), \quad (\text{B3})$$

where $P_a = P_{na}$ and $P_f = P_{nf}$. From Eqs. (B1) and (B2), we can easily get

$$N_m P_g = \bar{\Theta} \gamma_{\text{pl}} \mathcal{N}_{\text{pl}} + N_m k_{f \rightarrow g} k_{e \rightarrow f} \bar{\Theta} \bar{\Theta}, \quad (\text{B4})$$

$$N_m P_e = -\bar{\Xi} \gamma_{\text{pl}} \mathcal{N}_{\text{pl}} + N_m k_{f \rightarrow e} k_{g \rightarrow f} \bar{\Xi} \bar{\Xi}. \quad (\text{B5})$$

Using $P_f = 1 - P_g - P_e$ and inserting Eqs. (B4) and (B5) in Eq. (B3), we get the Eq.(25) in the main text.

Appendix C: Derivation of Rate Equations

The equations of motion for the populations $P_{na} \equiv \text{tr}_S \{ \hat{\rho}(t) |a_n\rangle \langle a_n| \}$ read

$$\frac{\partial}{\partial t} P_{ne} = -k_{e \rightarrow f}^{(n)} P_{ne} + k_{f \rightarrow e}^{(n)} P_{nf} - 2v_n \text{Im} \langle |g_n\rangle \langle e_n| C^+ \rangle \quad (\text{C1})$$

$$\frac{\partial}{\partial t} P_{ng} = -k_{g \rightarrow f}^{(n)} P_{ng} + k_{f \rightarrow g}^{(n)} P_{nf} + 2v_n \text{Im} \langle |g_n\rangle \langle e_n| C^+ \rangle \quad (\text{C2})$$

The correlations $\langle |g_n\rangle \langle e_n| C^+ \rangle \equiv \text{tr}_S \{ \hat{\rho}(t) |g_n\rangle \langle e_n| C^+ \}$ satisfy the following equation

$$\begin{aligned} \frac{\partial}{\partial t} \langle |g_n\rangle \langle e_n| C^+ \rangle = & i(\tilde{\omega}_{\text{pl}}^* - \tilde{\omega}_n) \langle |g_n\rangle \langle e_n| C^+ \rangle \\ & + iv_n (P_{ne} + \langle (|e_n\rangle \langle e_n| - |g_n\rangle \langle g_n|) C^+ C \rangle) \\ & + i \sum_{n' \neq n} v_{n'} \langle |e_{n'}\rangle \langle g_{n'}| \times |g_n\rangle \langle e_n| \rangle, \end{aligned} \quad (\text{C3})$$

where the complex transition frequencies are defined as $\tilde{\omega}_{\text{pl}} = \omega_{\text{pl}} - i\gamma_{\text{pl}}/2$ and $\tilde{\omega}_n = \omega_n - i(k_{e \rightarrow f}^{(n)} + k_{g \rightarrow f}^{(n)})/2$. To obtain closed equations, we omit the short-lived correlations involving two molecules in Eq. (C3). At steady state, we obtain

$$\langle |g_n\rangle \langle e_n| C^+ \rangle = \frac{iv_n}{\tilde{\omega}_{\text{pl}}^* - \tilde{\omega}_{eg}} \times (P_{ne} + (P_{ne} - P_{ng}) \langle C^+ C \rangle) \quad (\text{C4})$$

by assuming the factorization $\langle (|e_n\rangle \langle e_n| - |g_n\rangle \langle g_n|) C^+ C \rangle = (P_{ne} - P_{ng}) \langle C^+ C \rangle$. Inserting Eq. (C4) in Eqs. (C1) and (C2), we obtain Eqs. (27) and (28) in the main text.

-
- [1] Y. Yin, T. Qiu, J. Li, P. K. Chu, *Nano Energy* **1**, 25 (2012)
 - [2] P. Berini and I. D. Leon, *Nature Pho.* **6**, 16-24 (2012)
 - [3] M. A. Noginov, G. Zhu, A. M. Belgrave, et al, *Nature* **460**, 1110-1112 (2009)
 - [4] X. G. Meng, A. V. Kildishev, K. Fujita, et al., *Nano Lett.* **9**, 4106 (2013)
 - [5] Y. J. Lu, J. Kim, H. Y. Chen, et al., *Science* **337**, 450 (2012)
 - [6] W. Zhou, M. Dridi, J.Y. Suh, C.H. Kim, D.T. Co, M.R. Wasielewski, G.C. Schatz, and T.W. Odom, *Nature Nanotech.* **8**, 506-511 (2013)

- [7] A. Yang, T.B. Hoang, M. Dridi, C. Deeb, M.H. Mikkelsen, G.C. Schatz, and T.W. Odom, *Nature Comm.* **6**, 1-7 (2015)
- [8] C. Zhang, Y. H. Lu, Y. Ni, M. Z. Li, L. Mao, C. Liu, D. G. Zhang, H. Ming, and P. Wang, *Nano. Lett.* **15**, 1382 (2015)
- [9] R. M. Ma, R. F. Oulton, V. J. Sorger, G. Bartal, X. Zhang, *Nature Mat.* **10**, 110 (2011)
- [10] C. Y. Wu, C. T. Kuo, C. Y. Wang, et al., *Nano Lett.* **11**, 4256 (2011)

- [11] Y. J. Lu, C. Y. Yang, J. Kim, et al, Nano Lett. **14**, 4381 (2014)
- [12] Q. Zhang, G. Y. Li, X. F. Liu, F. Qian, Y. Li, T. C. Sum, C. M. Lieber and Q. H. Xiong, Nature Comm. **5**, 4953 (2014)
- [13] K. Ding, Z. C. Liu, L. J. Yin, et al., Phys. Rev. B **85**, 041301(R) (2012)
- [14] M. T. Hill, M. Marell, E. S. P. Leong, et al., Opt. Express **17**, 11107 (2009)
- [15] M. I. Stockman, J. Opt. **12**, 02404 (2010)
- [16] G. Kewes, R. R. Oliveros, K. Höfner, A. Kuhlicke, O. Benson, K. Busch, arXiv: **1412**. 4549 (2015)
- [17] Y. Zhang, and V. May, J. Chem. Phys. **142**, 224702 (2015)
- [18] Y. Zhang, and V. May, Phys. Rev. B **89**, 245441 (2014)
- [19] V. N. Pustovit, A. M. Urbas, A. Chipouline, and T. V. Shahabazyan, arXiv:1002.00612v1
- [20] A. S. Rosenthal and T. Ghannam, Phys. Rev. A **79**, 043824 (2009)
- [21] I. E. Protsenko, A. V. Uskov, O. A. Zaimidoroga, V. N. Samoilov, and E. P. O'Reilly, Phys. Rev. A **71**, 063812 (2005)
- [22] S. W. Chang, C. A. Ni, and S. L. Chuang, Opt. Exp. **16**, 10580 (2008)
- [23] S.W. Chang, S. L. Chuang, IEEE **45**, 1014, (2009)
- [24] V. M. Parfenyev and S. S. Vergeles, Phys. Rev. A **86**, 043824 (2012)
- [25] V. M. Parfenyev and S. S. Vergeles, Opt. Exp. **22**, 13571 (2014)
- [26] M. Richter, M. Gegg, T. S. Theuerholz, and A. Knorr, Phys. Rev. B **91**, 035306 (2015)
- [27] F. J. Duarte, L. S. Liao and K. M. Vaeth, Opt. Lett. **30**, 3072 (2005)
- [28] K. Hayashi, H. Nakanotani, M. Inoue, et al., App. Phys. Lett. **106**, 093301 (2015)
- [29] U. Martini, *Cavity-QED with many atoms*, Phd thesis, Ludwig-Maximilians-University Munich, Germany (2000)
- [30] S. E. Harris, Phys. Rev. Lett. **62**, 1033 (1989)
- [31] M. Xu, D. A. Tieri, and M. J. Holland, arXiv:1302.6284v2 (2013)
- [32] L. Mandel, and E. Wolf, *Optical coherence and quantum optics*, (Cambridge University Press, Cambridge, 1995) p840
- [33] J. H. Wesenberg, A. Ardavan, G. A. D. Briggs, J. J. L. Morton, R. J. Schoelkopf, D. I. Schuster, and K. Mølmer, Phys. Rev. Lett. **103** 070502 (2009)
- [34] Z. Kurucz, J. H. Wesenberg, K. Mølmer, Phys. Rev. A **83**, 053852 (2011)
- [35] B. A. Chase, J. M. Geremia, arXiv:0805.2910 (2013)
- [36] V. May, O. Kühn, Phys. Rev. B **77**, 115439 (2008)
- [37] V. May, O. Kühn, Phys. Rev. B **77**, 115440 (2008)
- [38] S. W. Wu, G. V. Nazin, and W. Ho, Phys. Rev. B **77**, 205430 (2008)
- [39] Y. Zhang, Y. Zelinskyy, and V. May, J. Phys. Chem. C **116**, 25962 (2012)
- [40] Y. Zhang, Y. Zelinskyy, and V. May, Phys. Rev. B **88**, 155426 (2013)
- [41] Y. Zhang, Y. Zelinskyy and V. May, J. Nanophotonics **6**, 063533 (2012)
- [42] M. Sargent II, M. O. Scully and W. E. Lamb, *Laser Physics* (Addison-Wesley Publishing Company, London, 1974)
- [43] W. Vogel and D. G. Welsch, *Lectures on Quantum Optics* (Akademie Verlag/VCH Publishers, Berlin/New York, 1994)
- [44] G. Weick, G. L. Ingold, R. A. Jalabert, and D. Weinmann, Phys. Rev. B **74**, 165421 (2006)
- [45] P. Meystre, and M. Sargent, *Elements of Quantum Optics*, (Springer-Verlag, Berlin, 1990)
- [46] Y. Zhang, and K. Mølmer, Quantum laser theory with three-level emitters under coherent optical pumping, in preparation
- [47] Heisenberg's uncertainty principle says that the time uncertainty Δt multiplied by the energy uncertainty ΔE should be larger than Planck constant \hbar : $\Delta t \times \Delta E \geq \hbar$. For the molecular junction, we relate Δt with the life-time of the lead plasmon and ΔE with the uncertainty ΔE_{pl} of the plasmon excitation energy E_{pl} . Since the energy E_{photon} of emitted photons is determined by E_{pl} , the uncertainty of the photon energy ΔE_{photon} , i.e. the emission line-width, is identical to ΔE_{pl} . Because the plasmon damping is compensated by the excited molecules, indicated by the increased plasmon mean number, the plasmon life-time becomes longer. Therefore, the emission line-width is reversely proportional to the plasmon mean number or the emission intensity.